Molecular Imaging
Volume 17: 1-9
© The Author(s) 2018
Article reuse guidelines:
sagepub.com/journals-permissions
DOI: 10.1177/1536012118799131
journals.sagepub.com/home/mix
SAGE

Rare-Earth-Doped Nanoparticles for Short-Wave Infrared Fluorescence Bioimaging and Molecular Targeting of $\alpha_v\beta_3$-Expressing Tumors

Dominik Jan Naczynski, PhD[1], Jason H. Stafford, PhD[1], Silvan Türkcan, PhD[1], Cesare Jenkins, PhD[1], Ai Leen Koh, PhD[2], Conroy Sun, PhD[1,3], and Lei Xing, PhD[1]

Abstract

The use of short-wave infrared (SWIR) light for fluorescence bioimaging offers the advantage of reduced photon scattering and improved tissue penetration compared to traditional shorter wavelength imaging approaches. While several nanomaterials have been shown capable of generating SWIR emissions, rare-earth-doped nanoparticles (REs) have emerged as an exceptionally bright and biocompatible class of SWIR emitters. Here, we demonstrate SWIR imaging of REs for several applications, including lymphatic mapping, real-time monitoring of probe biodistribution, and molecular targeting of the $\alpha_v\beta_3$ integrin in a tumor model. We further quantified the resolution and depth penetration limits of SWIR light emitted by REs in a customized imaging unit engineered for SWIR imaging of live small animals. Our results indicate that SWIR light has broad utility for preclinical biomedical imaging and demonstrates the potential for molecular imaging using targeted REs.

Keywords

cancer detection imaging, advances in optical probes, SWIR, short-wave infrared, NIR-II, nanoparticle, near-infrared imaging, integrin

Introduction

Imaging approaches that are able to resolve the physiological and molecular complexity of cancer can provide deep insight into the underlying causes of disease development, improve our understanding of treatment responses, and ultimately lead to better patient prognoses.[1-3] Molecular imaging approaches, in particular, offer a means by which to monitor the dynamics of cancer progression, permitting their use in a wide variety of clinical applications ranging from assessment of tumor metabolism to in situ molecular profiling.[4-6] However, current imaging efforts are limited by the availability of contrast agents with the requisite properties for enabling rapid resolution of molecular features within biological tissue. In contrast to other molecular imaging modalities, optical imaging offers remarkable detection sensitivity and the ability to conduct real-time image acquisition.[7-9] Traditionally, optical imaging has relied on the use of visible or near-infrared (NIR) light. Photons in these spectral regions are heavily scattered as they pass through biological tissue and produce background autofluorescence generated by tissue components. These limitations result in limited photon penetration, poor image resolution, and a low signal to noise ratio for distinguishing targets of interest.[10-12] In contrast, recent reports describing imaging with NIR-II or short-wave infrared (SWIR) light have shown this spectral region (1000-2300 nm) exhibiting reduced light scattering, improved photon penetrance, and exceptionally low autofluorescence.[13-15]

Various materials have been investigated as NIR-II emitting agents, including single-walled carbon nanotubes (SWNTs),[16-21]

[1] Department of Radiation Oncology, Stanford University School of Medicine, Palo Alto, CA, USA
[2] Stanford Nanocharacterization Laboratory, Stanford University, Palo Alto, CA, USA
[3] Department of Pharmaceutical Sciences, Oregon State University, Corvallis, OR, USA

Submitted: 11/06/2017. Revised: 22/06/2018. Accepted: 04/08/2018.

Corresponding Author:
Lei Xing, Department of Radiation Oncology, Stanford University School of Medicine, Palo Alto, CA 94305, USA.
Email: lei@stanford.edu

quantum dots,[22-24] small-molecule fluorophores,[25-27] and rare-earth-doped nanoparticles (REs).[13,28] While each class of agents offer certain advantages for in vivo imaging, REs have emerged as a versatile nanomaterial platform exhibiting bright SWIR emissivity, favorable biocompatibility, and tunable emission characteristics.[29-31] Rare-earth-doped nanoparticles are typically composed of a fluoride-based nanocrystal host that has been doped with one or more rare-earth cations. Unlike the broad emissions and low quantum yields observed with SWNTs,[14] REs produce bright SWIR emissions following NIR excitation with emission peaks that can be selected throughout the entire SWIR spectrum by careful selection of rare-earth elements during synthesis.[32,33] Rare-earth-doped nanoparticles have also been shown to be exceptionally resilient to photobleaching under prolonged excitation or exposure to ambient lighting conditions, which is ideal for repeated imaging in real time.[34]

Recent reports on the use of SWIR-emitting REs as in vivo imaging probes have focused on the detection of tumor lesions using untargeted, protein-modified REs and relied primarily on nanoparticle size to enhance tumor accumulation.[13] Subsequent work reported SWIR in vivo imaging using REs decorated with physically adsorbed targeting agents.[28] The focus of our current work was to investigate whether REs could be utilized as SWIR molecular imaging probes by targeting these agents to a specific tumor biomarker. We chose to further explore the use of REs in several other proof-of-concept SWIR bioimaging applications including lymphatic mapping and tracking probe biodistribution.

Methods

Synthesis and Functionalization of Rare-Earth Nanoparticles

NaYF4: Er, Yb nanoparticles were prepared using a well-established solvothermal decomposition method. Briefly, rare-earth trifluoroacetate precursors were dissolved in oleylamine. The shell precursor solution was prepared by dissolving stoichiometric amounts of the sodium and yttrium trifluoroacetates in oleylamine. The core solution was heated to 340°C under vigorous stirring in inert nitrogen atmosphere to allow the formation of the core. Next, the shell precursor was added, and after cooling, the synthesized nanoparticles were precipitated out of solution and washed repeatedly with ethanol. The resulting REs were surface modified with 1,2-distearoyl-sn-glycero-3-phosphoethanolamine-N-(amino[polyethylene glycol]-2000) 1,2-distearoyl-sn-glycero-3-phosphoethanolamine-N-[amino(polyethylene glycol)-2000] (DSPE-PEG(2000) amine) –polyethylene glycol (PEG)–NH_2 (MW 2000; Avanti Polar Lipids, Alabaster, Alabama) by ligand exchange performed in tetrahydrofuran (THF) under ultrasonication (Branson Ultrasonic Corp, Danbury, Connecticut). Polyethylene glycolylated REs were then added dropwise into deionized water and excess THF was evaporated overnight under gentle heating (40°C). Any remaining aggregates were removed by a 0.22-μm filter.

Rare-earth-doped nanoparticles were functionalized with cyclized tripeptide Arginine-glycine-aspartic acid (RGD) or Arginine–alanine–aspartate (RAD) (Peptides International, Louisville, Kentucky), for targeting studies. Peptide conjugation was performed through covalent attachment to the amine-functionalized nanoparticles using N-hydroxysuccinimide heterobifunctional linkers and thiolation chemistry. Succinimidyl iodoacetate (10 mg; Pierce Biotechnology, Waltham, Massachusetts) was dissolved into 0.1 mL of dimethyl sulfoxide and added to the 1.0 mL of the PEGylated nanoparticle suspension described in the previous section. The solution was protected from light and placed on a shaker for 2 hours at room temperature. The nanoprobes were purified by Zeba spin columns (40 K MWCO; Pierce Biotechnology) eluted with 100 mM bicarbonate buffer (pH 8.50). Next, 1.0 mg of the purified iodoacetate functionalized nanoparticles was added to either Cys-modified cyclic RGD or cyclic RAD for 2 hours at room temperature. Upon conjugation, the peptide-conjugated nanoparticles were purified by column chromatography using Zeba spin columns against phosphate-buffered saline (PBS).

Nanoparticle Characterization

Rare-earth-doped nanoparticles were visualized by transmission electron microscopy (TEM). Transmission electron microscopy grids were prepared by depositing a drop of diluted nanoparticle suspension on ultrathin carbon support film (Ted Pella, Redding, California). All TEM measurements were acquired using an FEI 80-300 Titan operated at 300 kV. Electron dispersive spectroscopy measurements are acquired in TEM mode, with the beam focused down to the size of an individual particle.

Hydrodynamic size was measured in PBS using Zetasizer Nano series dynamic light scattering (DLS) particle size analyzer (Malvern Instruments, Malvern, UK). Emission spectra of REs were collected from a dried pellet ($\sim$0.5 g) of nanoparticles following exposure to NIR light generated from a 975 nm laser diode (B&W Tek, Newark, Delaware). Spectra were collected using a spectrometer (Princeton Instruments, Trenton, New Jersey) coupled to an InGaAs detector.

Short-Wave Infrared Imaging System

A custom small animal imaging system was designed to capture low levels of SWIR light. The system was housed within a light, tight black box equipped with a moveable stage and tubing ports for convenient administration of isoflurane and removal of waste gas. An InGaAs camera (NIRvana 640; Princeton Instruments) with >80% quantum efficiency in the desired SWIR emission range was positioned above the imaging plane. A Schneider Xenon lens (F-number: 0.95, focal length: 17 mm) was installed onto the camera and equipped with a combination of one 1400 nm long-pass (FEL1400; ThorLabs, Newton, New Jersey) and two 1550 nm

(FB1550-12; ThorLabs) bandpass filters. A 975 nm laser source was piped into the black box through a fiber optic cable, which was attached to a collimator and diffuser to enable a uniform and constant excitation beam radius. Acquired SWIR images were processed using ImageJ (version 1.48).

Cell Culture

U87-luc, a human glioblastoma cell line with constitutive expression of firefly luciferase, was generously provided by Dr Prabhas Moghe (Department of Biomedical Engineering, Rutgers University). Cells were maintained in minimal essential medium containing 10% fetal bovine serum (FBS) G418 (300 mg·mL^{-1}), and 1% penicillin–streptomycin. 4T1, MDA-MB-231, and MCF-7 breast cancer cell lines were all maintained in RPMI media containing 10% FBS and 1% penicillin–streptomycin. All cells were cultured at 37°C under an atmosphere of 5% CO_2.

Cell Targeting

Two human breast cancer cell lines with varied expression of the $\alpha_v\beta_3$ were chosen to assess the in vitro cellular targeting of functionalized REs. High $\alpha_v\beta_3$ expressing MDA-MB-231 and low $\alpha_v\beta_3$ expressing MCF-7 cells were seeded at 10^5 cells per well in a 6-well plate (at least a 20-fold difference in expression).[35] After 24 hours postseeding, approximately 10 μg/mL of RGD- or RAD-functionalized REs was added to the media of MDA-MB-231 and MCF-7 cells. Following 2 hours of incubation, media was replaced and cells were washed 3× in PBS before trypsinization. Cell suspensions were pelleted and imaged for SWIR fluorescence using the SWIR imaging system.

In vivo SWIR Imaging

All animal studies were conducted in accordance with Stanford University Institutional Animal Care and Use Committee–approved protocols. During imaging experiments, animals were weighed daily and monitored for changes in behavior. Imaging was performed on 8-week-old female athymic nude mice purchased from Charles River Laboratories (San Diego, California). For biodistribution imaging, 50 μL of 2.5×10^6 4T1 cells mixed with 50 μL of Matrigel were subcutaneously injected into the mammary fat pad. For nanoparticle targeting imaging, 50 μL of 2.5×10^6 U87-luc cells mixed with 50 μL of Matrigel were subcutaneously injected into the right flank. Tumor diameters were measured twice weekly with electronic calipers and tumor volumes calculated by the formula: volume $= (d_{short})^2 \times (d_{long})/2$, where d_{short} and d_{long} represent the short and long diameters, respectively. Tumors were allowed to grow to 100 mm^3 prior to initiating the SWIR imaging studies.

To assess the location of tumor burden for the targeted imaging studies, U87-luc tumor margins were confirmed with bioluminescence imaging captured after intraperitoneal injection of mice with 100 μL of 30 mg/mL of d-luciferin. Bioluminescence imaging was carried out in a biological irradiator equipped with an EMCCD (Precision X-Ray Inc, North Branford, Connecticut), which simultaneously acquired X-ray images of the animal for anatomical correlation of the bioluminescence signal. After validation of tumor presence, background images of SWIR fluorescence were taken using the custom SWIR imaging system. Next, 150 μL of a 1 mg/mL solution of functionalized REs resuspended in PBS was intravenously injection into the tail vein, and SWIR imaging was performed at baseline, 30 minutes, 4 hours, 8 hours, 24 hours, 48 hours, and 120 hours. During a typical imaging session, mice were sedated under isoflurane and imaged under approximately 0.15 W/cm^2 of collimated 975 nm light. Short-wave infrared emissions were captured with the InGaAs camera operating with a 1-second integration time.

Short-wave infrared signal quantification was performed by matching the perimeter of tumor bioluminescence to the acquired SWIR fluorescence images. Average signal intensity as a function of time was measured in the tumors of all animals. These regions of interest were also positioned on nearby, untargeted muscle to acquire a background, nonspecific SWIR signal. Tumor to background ratios were calculated by dividing both these values for each time point and animal.

For the lymphatic mapping studies, 10 μL of a 20 mg/mL solution of PEGylated REs was subcutaneously administered into the forepaw of nude mice. Short-wave infrared imaging was performed to track nanoparticle drainage over 15 minutes. All mice were anesthetized with an intraperitoneal injection of a ketamine hydrochloride and xylazine cocktail prior to imaging.

Measurement of Optical Attenuation and Resolution

Phantom tissue composed of scattering and absorbing agents was used to assess the limits of signal detection and resolution. Phantom tissue was composed of 1% agarose, 1% Intralipid (Sigma-Aldrich, Milwaukee, Wisconsin) and 170 μM hemoglobin. Increasing thickness of tissue was layered over a hot spot resolution phantom (Micro Deluxe Phantom; Data Spectrum Corporation, Durham, North Carolina) with approximately 0.1 g of REs pressed into its chambers. Short-wave infrared imaging was subsequently performed through the phantom tissue.

Results and Discussion

Rare-earth-doped nanoparticles were first synthesized according to a well-established thermal decomposition method and were composed of an ytterbium (Yb)- and erbium (Er)-doped NaYF4 core surrounded by an undoped NaYF4 shell.[36] Rare-earth doped nanoparticles exhibited uniform morphology under TEM imaging (Figure 1A) and were approximately 17.1 ± 3.1 nm in diameter (Figure 1B), as measured by DLS. In contrast to Er and Yb-doped Y2O3 nanoparticles,[37] REs exhibited a significantly smaller diameter, a key physical

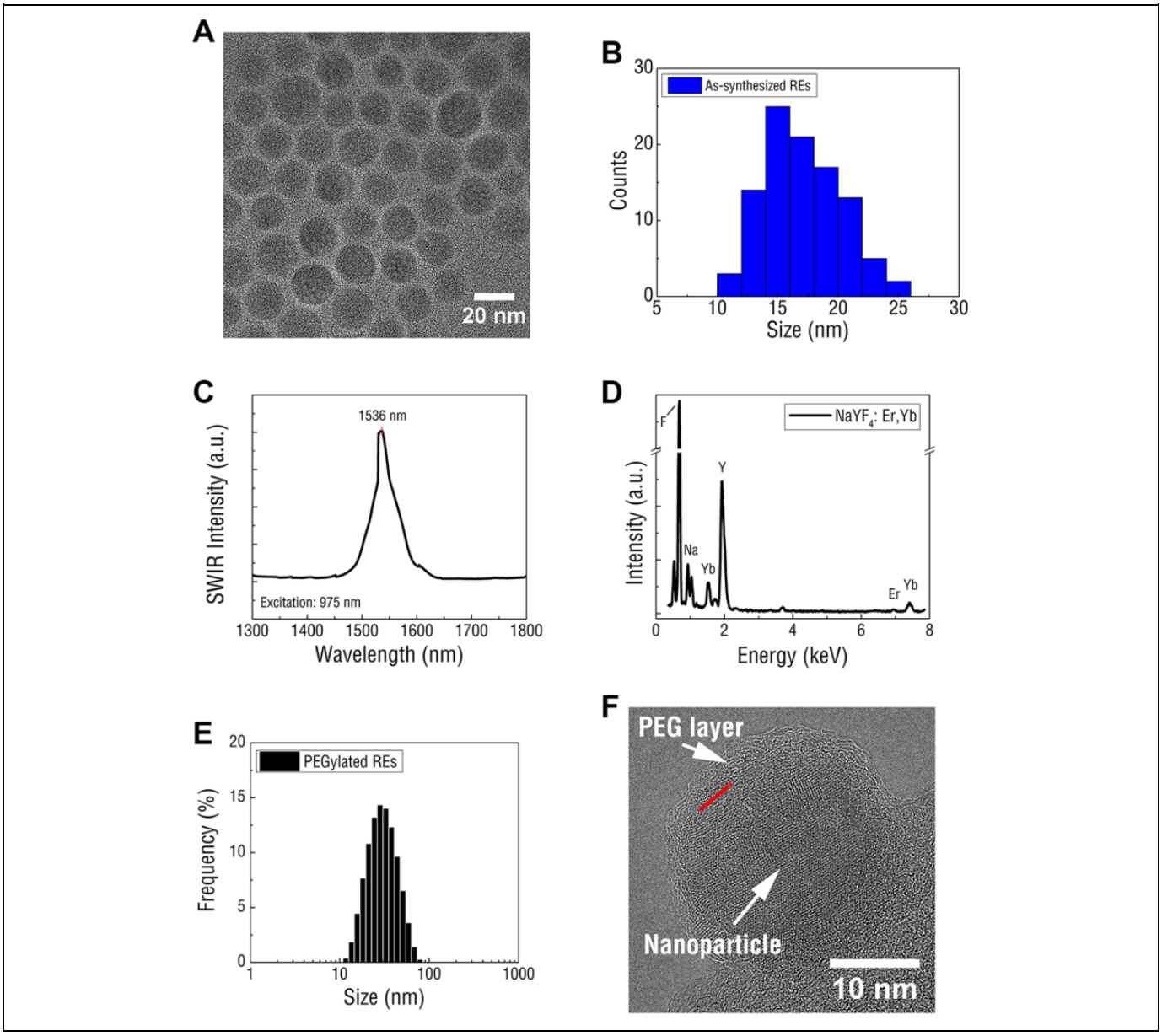

Figure 1. A, Rare-earth-doped nanoparticles display spherical morphology and homogenous size distribution as shown by TEM. B, Dynamic light scattering confirms uniform RE particle size distribution. C, Upon NIR excitation at 975 nm, REs displayed bright, narrow emission at 1536 nm. D, energy dispersive X-ray spectroscopy (EDS) profile of REs confirm the elemental composite of the NaYF4 nanoparticles and confirm the presence of Er, the rare-earth dopant and SWIR emitter. E, polyethylene glycolylated REs display narrow size distribution in aqueous solution and are noticeably larger in diameter than assynthesized Res. F, Transmission electron microscopy imaging of PEGylated REs show a crystalline nanoparticle encased in an amorphous shell with the boundary indicated by the red line. DLS indicates dynamic light scattering; NIR, near infrared; PEG, polyethylene glycol; RE, rare-earth doped nanoparticles; SWIR, short-wave infrared; TEM, transmission electron microscopy; YF, yttrium fluoride.

parameter for ensuring an acceptable pharmacokinetic properties.[38] Upon excitation with 975 nm NIR light, a relatively narrowband of SWIR emission was observed with λ_{max} at 1535 nm near the anticipated emission peak of the Er dopant (Figure 1[c]). Qualitative analysis of RE atomic composition through energy-dispersive X-ray spectroscopy confirmed the predicted dopant concentrations of 20% Yb and ~2% Er (Figure 1[d]). The observed lattice fringes were indicative of a predominately hexagonal (β) phase crystalline structure, which has been previously described as the optimal phase for enabling efficient SWIR emissivity.[33]

Rare-earth doped nanoparticles were prepared for in vitro and in vivo testing by exchanging surface-bound surfactant remaining from synthesis with PEG through ultrasonication. In contrast to unmodified REs, PEG-coated REs were stable in aqueous solution (Supplemental Figure S1) and exhibited relatively small hydrodynamic diameters (mean = 34 nm) in aqueous solution (Figure 1[e]). Transmission electron

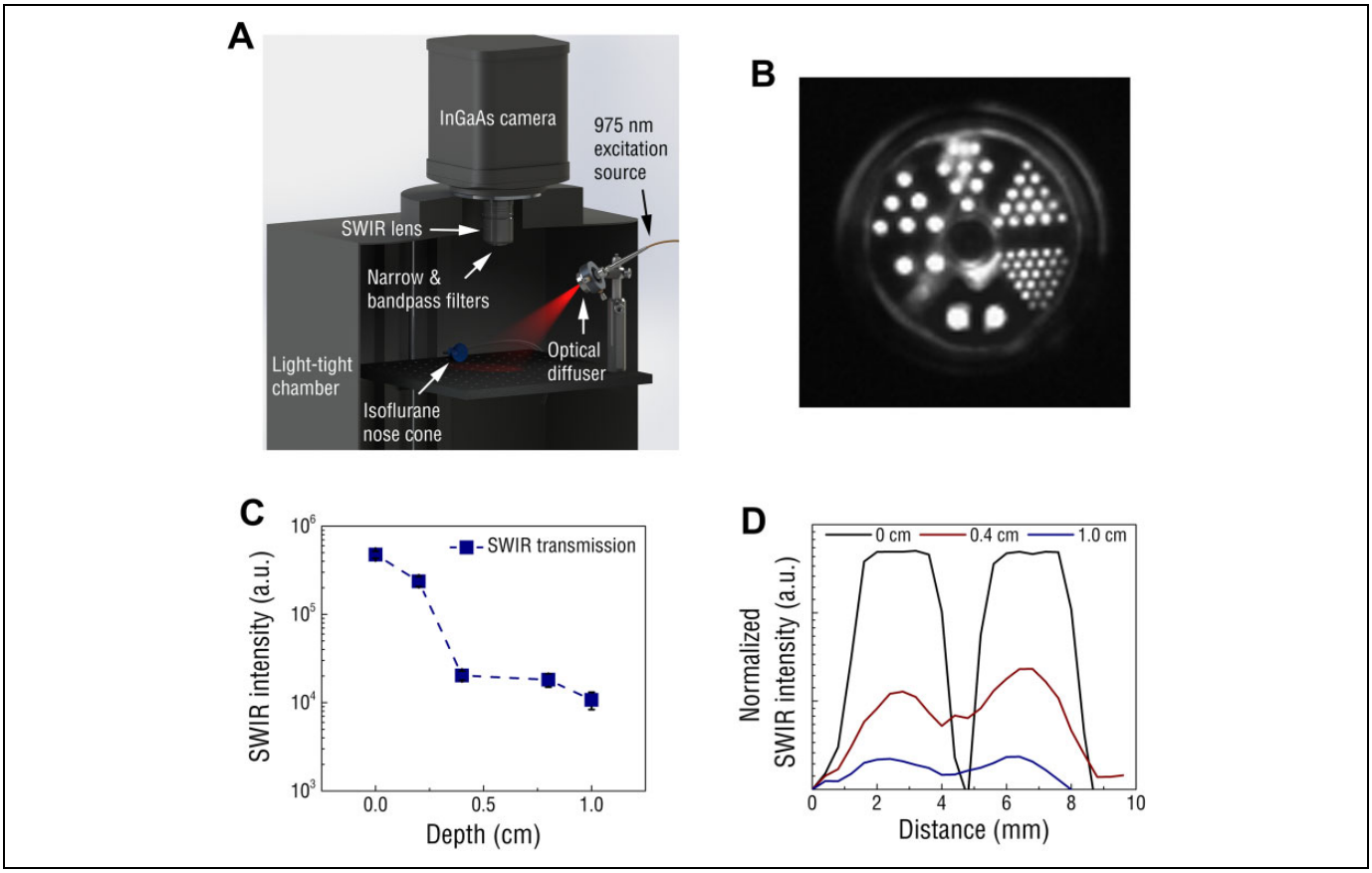

Figure 2. A, Schematic of the small animal SWIR imaging system. B, PET chamber filled with REs and excited at 975 nm. Rod diameters counterclockwise from bottom are 4.8 mm, 4.0 mm, 3.2 mm, 2.4 mm, 1.6 mm, and 1.2 mm. C, Short-wave infrared signal from REs progressively diminished through increasing depth of phantom tissue, yet signal was still detected through 1.0 cm of tissue. D, Effects of increasing phantom depth on the SWIR resolution reveals point fluorescence could be distinguished with millimeter precision using the 4.8-mm-diameter rods as SWIR emission points. RE indicates rare-earth-doped nanoparticles; SWIR, short-wave infrared.

microscopy imaging validated the DLS results, revealing individual REs encased in an amorphous coating that likely corresponded to the PEG (Figure 1[f]).

A custom SWIR imaging system was engineered and used for assessing the imaging capabilities of REs (Figure 2[a]). The signal detection limits of the SWIR imaging system were established using serial dilutions of REs. Short-wave infrared emission intensity correlated linearly ($r^2 = 0.992$) with RE concentration (Supplemental Figure S2), and the lowest detectable concentration of REs was found to be in the single-digit nanomolar range (assuming an RE molecular weight of 7×10^6 g/mol based on an average diameter of 17 nm and density of 4.21 g/cm^3 for bulk NaYF4).[39] Tissue-mimicking phantoms composed of scattering and absorbing agents were used to assess the limits of imaging resolution. A PET resolution chamber was filled with dried REs and irradiated through phantom tissue (Figure 2[b]). Short-wave infrared signal could be detected through up to 1 cm of tissue (Figure 2[c]), and at these depths, RE localization could be resolved at millimeter resolution (Figure 2[d]).

Early proof-of-concept SWIR imaging studies were conducted using PEGylated REs for lymphatic mapping and passive tumor targeting. To assess the in vivo resolving capabilities of SWIR, lymphatic imaging was performed using PEGylated REs injected into the footpads of mice. Short-wave infrared imaging revealed bright, concentrated emissions that diminished from the injection site and progressively travelled through the hind legs toward the abdomen (Figure 3[a]). Rare-earth doped nanoparticles were tracked through the lymphatic vasculature and could be resolved at $\sim$450 μm using the imaging platform (Figure 3[b, c]). Bright SWIR emissions were observed near the junction of the leg and abdomen 30 minutes postinjection, which corresponded to the nearest draining sentinel lymph nodes.

Additionally, tumor engraftment studies were used to evaluate the biodistribution of PEGylated REs and determine their potential for passive tumor accumulation. The mammary fat pads of athymic, nude mice were inoculated with a bolus of 4T1 breast cancer cells. Following tumor growth, PEGylated REs were intravenously injected into the animals and SWIR imaging was performed over time. After approximately 5 minutes, SWIR signal became concentrated throughout the animals, including in the tumor xenografts. Short-wave infrared emissions were detected in various organs throughout the

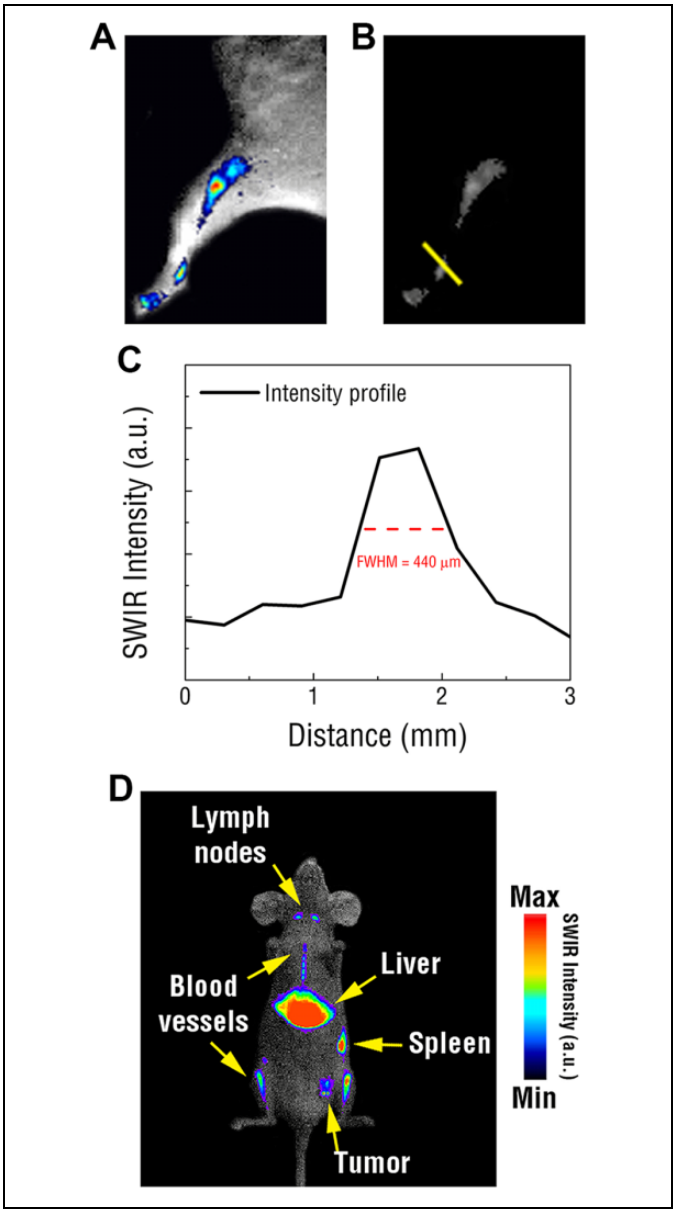

Figure 3. A, Representative image showing tracking of the lymphatic vascular in the hind leg of a mouse using REs injected into the footpad. B, Raw SWIR image used to assess the resolution of SWIR signal tracked through the lymphatic vasculature. C, Reveals submillimeter, micron resolution. D, Representative SWIR image of PEGylated REs intravenously injected into a mouse exhibiting a 4T1 tumor reveals intense SWIR emissions emitted from the liver, spleen, and lymph nodes as well as certain vasculature and passive tumor accumulation. RE indicates rare-earth doped nanoparticles; SWIR, short-wave infrared; PEG, polyethylene glycol.

animal, which were later identified to correspond to the liver, spleen, and lymph nodes following dissection (Figure 3[d]). Notably, SWIR emissions were readily identifiable within larger structures of the circulatory network, such as the aorta.

While passive targeting provides a convenient means to screen the tumor accumulation properties of nanoparticles in vivo, this approach lacks the required specificity to accurately profile the molecular characteristics of tumor burden in situ. To accomplish this, REs were engineered to target the $\alpha_V\beta_3$ receptor, which has been shown to be highly expressed in a wide variety of malignant tumors, including those of the brain, breast, and prostate.[40-42] Furthermore, expression of this receptor has been linked to the progression of tumor angiogenesis and may be correlated with greater tumor malignancy and poorer prognosis.[42-44] To enable targeting of the receptor, the surfaces of PEGylated REs were functionalized with the cyclic RGD tripeptide, a well-established antagonist of the $\alpha_v\beta_3$ integrin receptor.[45,46] Functionalization was achieved via covalent linkage of the tripeptide moiety to the REs. In contrast to previous work,[28] our approach binds the targeting moiety onto REs via a covalent linkage, which enables improved in vivo stability and provides greater control of targeting agent deposition.[47] The functionalization process used in our study is straightforward and broadly applicable to conjugating other targeting moieties with free thiol groups.

RGD-modified REs (RGD-REs) were found to be approximately 127 $\pm$ 5 nm in PBS, approximately 100 nm larger when compared to nonfunctionalized, PEGylated REs (Supplemental Figure S3). To determine whether functionalized REs retained the molecular binding characteristics of soluble RGD, RGD-REs were exposed to both a highly and weakly $\alpha_v\beta_3$ integrin expressing cell line. High expressing MDA-MD-231 breast cancer cells exposed to RGD-REs were found to exhibit significantly greater SWIR fluorescence intensity than low $\alpha_v\beta_3$ expressing MCF-7 breast cancer cells at comparable exposure concentrations (Figure 4[a]). In contrast, there was little detectable SWIR emission from any of the cell lines exposed to a REs functionalized with RAD (RAD-REs), a tripeptide sequence used as a negative control. Rare-earth-doped nanoparticles functionalized with RAD displayed similar size distribution and SWIR signal emissivity as their RGD counterparts.

To assess the ability of functionalized REs to preferentially target tumors expressing a molecular biomarker, RGD and RAD functionalized REs were intravenously administered in athymic nude mice inoculated with a bolus of luciferase expressing U87 (U87-luc) cells (Figure 4[b]). Similar to the naive U87 cell line, U87-luc cells exhibit high expression of the $\alpha_v\beta_3$ integrin receptor. Bioluminescence imaging was performed to confirm tumor presence and establish tumor margins of the U87-luc xenografts on each animal. In parallel, X-ray, white light imaging, and back-lit SWIR imaging were performed to establish an anatomical reference for the tumor mass. Following injection of functionalized REs, SWIR fluorescence was observed throughout the animals. Most prominently, SWIR signal was observed in the livers confirming our previous observation of RE accumulation through passive targeting. Additionally, SWIR signal was observed near the base of the tail likely representing residue from the excretion of REs. Short-wave infrared signals were also observed in tumors at time points shorter than 24 hours following injection with either formulation. However, SWIR emissions at the site of tumors on mice injected with RGD-REs were found to

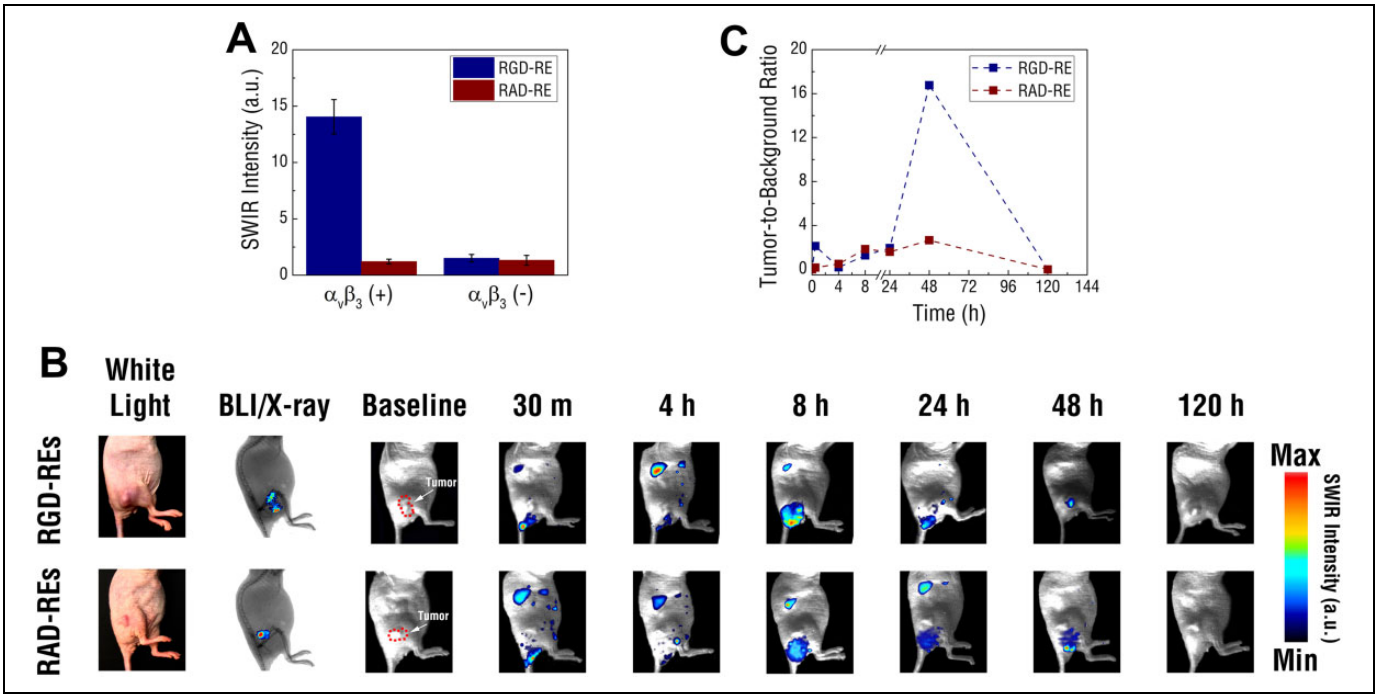

Figure 4. A, Targeting the $\alpha_v\beta_3$ receptor using RGD and RAD functionalized REs. Targeting of functionalized REs was first assessed and quantified in vitro using MDA-MB-231 and MCF-7 cell lines exhibiting varying expression of $\alpha V\beta 3$. B, Short-wave infrared signal was captured using the small animal imaging system and tracked over 120 hours. C, Bioluminescence and X-ray imaging were used to identify location of the luciferase expressing U87 tumor xenografts in relation to the mouse's anatomy. While SWIR signals were broadly distributed throughout the animals' bodies at earlier time points before being cleared at 120 hours, tumors in mice injected with RGD-REs showed enhancement of SWIR at 48 hours. Compared to background tissue, RGD-REs showed over a 15-fold signal enhancement compared to tumors in mice injected with RAD-REs (mean values $\pm$ SEM; n = 3; *P < .01) determined by Student t test; A). RE indicates rare-earth doped nanoparticles; SEM, standard error of mean; SWIR, short-wave infrared.

progressively increase in intensity with maximal signal observed approximately 48 hours postinjection. In contrast, mice injected with RAD-REs displayed significantly fainter SWIR signal in tumor regions signifying less effective targeting.

Tumor to background calculations indicated that injection of the RGD-RE formulation resulted in an approximately 6-fold greater tumor contrast than that observed by RAD-REs (Figure 4[c]). There was no measureable background SWIR fluorescence from the animal prior to the injection of the RE formulations. These results confirm that RGD-REs were able to preferentially target $\alpha_v\beta_3$ expressing U87-luc tumors and underscore the potential use of these agents for imaging molecular biomarkers of clinical significance using SWIR light.

An important consideration in the development of a biological contrast agent is its toxicity profile. The animal studies performed here revealed no apparent adverse effects or significant changes in animal weight following injection, though a trend in weight loss (range: 0%-5%) was observed after 5 days (Supplemental Figure S4). Furthermore, complete clearance of both formulations was captured by SWIR imaging and observed 120 hours postinjection. Although further experiments are necessary to validate these findings, our results support the conclusions of others that REs systemically injected into mice do not result in overt toxicity over the course of several days.[48] More comprehensive toxicity studies are planned in order to fully assess the safety profile of these agents.

The results presented here demonstrate the SWIR imaging capabilities of molecularly targeted REs. Nevertheless, the use of these agents for biomedical imaging will depend on both the maximum imaging depth that can be achieved and image resolution. Using our current imaging approach, we achieved a maximum imaging depth of approximately 1 cm and were able to resolve anatomical features at micron resolution. However, as detection depth is a function of contrast-agent concentration, excitation power density, tissue composition, and detector sensitivity, we anticipate that further improvements in both the SWIR imaging system and nanoparticle formulation will enable deeper signal detection and enhancement resolution. Our current results provide strong rationale for utilizing SWIR for various subsurface imaging applications, such as the assessment of cancer metastasis into lymphatic tissue. In the context of cytoreductive surgical procedures, such imaging approaches could ultimately result in better patient prognoses by ensuring the complete removal of malignant tissue and providing rapid molecular characterization of disease severity.

In the near-term, SWIR may find broader use in preclinical studies where imaging at centimeter depth could be sufficient to visualize molecular targets within small animal subjects.

Incorporating SWIR with other advanced optical imaging approaches, such as 3D fluorescence molecular tomography, could also be used to offer greater insight into the spatiotemporal dynamics of disease progression. Furthermore, previous work has highlighted the ease of synthesizing REs with unique SWIR emissivity profiles by modifying the types of rare-earth dopants used, providing a route for developing SWIR as a multispectral molecular imaging modality.[13] Although not explored in our current study, it is reasonable to envision a "RE cocktail" consisting of an assortment of uniquely emitting REs individually functionalized with several targeting agents designed to interrogate multiple molecular targets simultaneously. Such an approach would aid in understanding the complex interactions that occur among multiple molecular targets during disease progression.

Conclusions

Realizing the promise of optical molecular imaging requires the development of novel contrast agents designed to both accurately and sensitively resolve the molecular characteristics of disease through living tissue. Traditionally, optical imaging has relied on the use of shorter wavelengths of light (<1000 nm) to detect contrast agent in vivo. However, recent reports have indicated that SWIR (NIR-II) light offers the advantage of reduced photon scattering and improved tissue penetration compared to shorter wavelength light. Contrast agents that are detectable by SWIR and engineered to target specific biomarkers could therefore be useful tools in understanding the molecular dynamics of disease deep within live tissue using optical approaches. Here, we demonstrate proof-of-concept molecular SWIR imaging of tumors expressing the $\alpha_V\beta_3$ integrin receptor using targeted RE nanoparticles. In addition, we showed that SWIR was able to resolve detailed anatomical features like lymphatic vasculature with high image fidelity and track probe biodistribution in real time, further supporting the development of SWIR as a new optical imaging modality. The studies conducted here expand the uses of SWIR-emitting REs for molecular in vivo imaging and open the possibility for the broader application of these materials in more advanced imaging techniques.

Declaration of Conflicting Interests

The author(s) declared no potential conflicts of interest with respect to the research, authorship, and/or publication of this article.

Funding

The author(s) disclosed receipt of the following financial support for the research, authorship, and/or publication of this article: NIBIB (1R01 EB016777), NCI (1R01 CA133474), NIGMS, (1R35 GM119839), and the US Department of Defense, Breast Cancer Research Program award W81XWH-11-1-0087.

Supplemental Material

Supplemental material for this article is available online.

References

1. Weissleder R, Pittet MJ. Imaging in the era of molecular oncology. *Nature*. 2008;452(7187):580–589. doi:10.1038/nature06917.
2. Willmann JK, van Bruggen N, Dinkelborg LM, Gambhir SS. Molecular imaging in drug development. *Nat Rev Drug Discov*. 2008;7(7):591–607. doi:10.1038/nrd2290.
3. Pysz MA, Gambhir SS, Willmann JK. Molecular imaging: current status and emerging strategies. *Clin Radiol*. 2010;65(7):500–516. doi:10.1016/j.crad.2010.03.011.
4. van Dam GM, Themelis G, Crane LM, et al. Intraoperative tumor-specific fluorescence imaging in ovarian cancer by folate receptor-alpha targeting: first in-human results. *Nat Med*. 2011; 17(10):1315–1319. doi:10.1038/nm.2472.
5. Schaafsma BE, Mieog JS, Hutteman M, et al. The clinical use of indocyanine green as a near-infrared fluorescent contrast agent for image-guided oncologic surgery. *J Surg Oncol*. 2011;104(3): 323–332. doi:10.1002/jso.21943.
6. Crane LM, Themelis G, Arts HJ, et al. Intraoperative near-infrared fluorescence imaging for sentinel lymph node detection in vulvar cancer: first clinical results. *Gynecol Oncol*. 2011; 120(2):291–295. doi:10.1016/j.ygyno.2010.10.009.
7. Pierce MC, Javier DJ, Richards-Kortum R. Optical contrast agents and imaging systems for detection and diagnosis of cancer. *Int J Cancer*. 2008;123(9):1979–1990. doi:10.1002/ijc.23858.
8. Frangioni JV. In vivo near-infrared fluorescence imaging. *Curr Opin Chem Biol*. 2003;7(5):626–634.
9. Vahrmeijer AL, Hutteman M, van der Vorst JR, van de Velde CJ, Frangioni JV. Image-guided cancer surgery using near-infrared fluorescence. *Nature reviews Clinical oncology*. 2013;10(9): 507–518. doi:10.1038/nrclinonc.2013.123.
10. Lim YT, Kim S, Nakayama A, Stott NE, Bawendi MG, Frangioni JV. Selection of quantum dot wavelengths for biomedical assays and imaging. *Mol Imaging*. 2003;2(1):50–64.
11. Smith AM, Mancini MC, Nie S. Bioimaging: second window for in vivo imaging. *Nat Nanotechnol*. 2009;4(11):710–711. doi:10.1038/nnano.2009.326.
12. He X, Gao J, Gambhir SS, Cheng Z. Near-infrared fluorescent nanoprobes for cancer molecular imaging: status and challenges. *Trends Mol Med*. 2010;16(12):574–583. doi:10.1016/j.molmed.2010.08.006.
13. Naczynski DJ, Tan MC, Zevon M, et al. Rare-earth doped biological composites as in vivo shortwave infrared reporters. *Nat Commun*. 2013;4:2199. doi:10.1038/ncomms3199.
14. Welsher K, Liu Z, Sherlock SP, et al. A route to brightly fluorescent carbon nanotubes for near-infrared imaging in mice. *Nat Nanotechnol*. 2009;4(11):773–780. doi:10.1038/nnano.2009.294.
15. Welsher K, Sherlock SP, Dai H. Deep-tissue anatomical imaging of mice using carbon nanotube fluorophores in the second near-infrared window. *Proc Natl Acad Sci U S A*. 2011;108(22): 8943–8948. doi:10.1073/pnas.1014501108.
16. Diao S, Hong G, Robinson JT, et al. Chirality enriched (12,1) and (11,3) single-walled carbon nanotubes for biological imaging. *J Am Chem Soc*. 2012;134(41):16971–16974. doi:10.1021/ja307966u.

17. Robinson JT, Hong G, Liang Y, Zhang B, Yaghi OK, Dai H. In vivo fluorescence imaging in the second near-infrared window with long circulating carbon nanotubes capable of ultrahigh tumor uptake. *J Am Chem Soc*. 2012;134(25):10664–10669. doi:10.1021/ja303737a.
18. Hong G, Lee JC, Robinson JT, et al. Multifunctional in vivo vascular imaging using near-infrared II fluorescence. *Nat Med*. 2012;18(12):1841–1846. doi:10.1038/nm.2995.
19. Hong G, Diao S, Chang J, et al. Through-skull fluorescence imaging of the brain in a new near-infrared window. *Nat Photonics*. 2014;8(9):723–730. doi:10.1038/nphoton.2014.166.
20. Hong G, Lee JC, Jha A, et al. Near-infrared II fluorescence for imaging hindlimb vessel regeneration with dynamic tissue perfusion measurement. *Circ Cardiovasc Imaging*. 2014;7(3):517–525. doi:10.1161/CIRCIMAGING.113.000305.
21. Diao S, Blackburn JL, Hong G, et al. Fluorescence imaging in vivo at wavelengths beyond 1500 nm. *Angew Chem Int Ed Engl*. 2015;54(49):14758–14762. doi:10.1002/anie.201507473.
22. Zhang Y, Hong G, Zhang Y, et al. Ag2 S quantum dot: a bright and biocompatible fluorescent nanoprobe in the second near-infrared window. *Acs Nano*. 2012;6(5):3695–702. doi:10.1021/nn301218z.
23. Hong G, Robinson JT, Zhang Y, et al. In vivo fluorescence imaging with Ag2 S quantum dots in the second near-infrared region. *Angew Chem Int Ed Engl*. 2012;51(39):9818–9821. doi:10.1002/anie.201206059.
24. Franke D, Harris DK, Chen O, et al. Continuous injection synthesis of indium arsenide quantum dots emissive in the short-wavelength infrared. *Nat Commun*. 2016;7:12749. doi:10.1038/ncomms12749.
25. Hong G, Zou Y, Antaris AL, et al. Ultrafast fluorescence imaging in vivo with conjugated polymer fluorophores in the second near-infrared window. *Nat Commun*. 2014;5:4206. doi:10.1038/ncomms5206.
26. Antaris AL, Chen H, Cheng K, et al. A small-molecule dye for NIR-II imaging. *Nat Mater*. 2016;15(2):235–242. doi:10.1038/nmat4476.
27. Sun Y, Qu CR, Chen H, et al. Novel benzo-bis(1,2,5-thiadiazole) fluorophores for in vivo NIR-II imaging of cancer. *Chem Sci*. 2016;7(9):6203–6207. doi:10.1039/c6sc01561a.
28. Zevon M, Ganapathy V, Kantamneni H, et al. CXCR-4 targeted, short wave infrared (SWIR) emitting nanoprobes for enhanced deep tissue imaging and micrometastatic cancer lesion detection. *Small*. 2015;11(47):6347–6357. doi:10.1002/smll.201502202.
29. Naczynski DJ, Tan MC, Riman RE, Moghe PV. Rare earth nanoprobes for functional biomolecular imaging and theranostics. *J Mater Chem B Mater Biol Med*. 2014;2(20):2958–2973. doi:10.1039/C4TB00094C.
30. Prodi L, Rampazzo E, Rastrelli F, Speghini A, Zaccheroni N. Imaging agents based on lanthanide doped nanoparticles. *Chem Soc Rev*. 2015;44(14):4922–4952. doi:10.1039/c4cs00394b.
31. Hemmer E, Venkatachalam N, Hyodo H, et al. Upconverting and NIR emitting rare earth based nanostructures for NIR-bioimaging. *Nanoscale*. 2013;5(23):11339–11361. doi:10.1039/c3nr02286b.
32. van Saders B, Al-Baroudi L, Tan MC, Riman RE. Rare-earth doped particles with tunable infrared emissions for biomedical imaging. *Optical Materials Express*. 2013;3:566–573. doi:10.1364/ome.3.000566.
33. Tan MC, Connolly J, Riman RE. Optical efficiency of short wave infrared emitting phosphors. *J Phys ChemC*. 2011;115:17952–17957. doi:10.1021/jp203735n.
34. Wu SW, Han G, Milliron DJ, et al. Non-blinking and photostable upconverted luminescence from single lanthanide-doped nanocrystals. *Proc Natl Acad Sci U S A*. 2009;106(27):10917–10921. doi:10.1073/pnas.0904792106.
35. Bauer K, Mierke C, Behrens J. Expression profiling reveals genes associated with transendothelial migration of tumor cells: a functional role for alphavbeta3 integrin. *Int J Cancer*. 2007;121(9):1910–1918. doi:10.1002/ijc.22879.
36. Yi GS, Chow GM. Water-soluble NaYF4: Yb, Er(Tm)/NaYF4/polymer core/shell/shell nanoparticles with significant enhancement of upconversion fluorescence. *Chem Mater*. 2007;19:341–343. doi:10.1021/cm062447y.
37. Zako T, Yoshimoto M, Hyodo H, et al. Cancer-targeted near infrared imaging using rare-earth ion-doped ceramic nanoparticles. *Biomater Sci*. 2015;3(1):59–64. doi:10.1039/c4bm00232 f.
38. Davis ME, Chen ZG, Shin DM. Nanoparticle therapeutics: an emerging treatment modality for cancer. *Nat Rev Drug Discov*. 2008;7(9):771–782. doi:10.1038/nrd2614.
39. Cheng L, Yang K, Zhang S, Shao M, Lee S, Liu Z. Highly-sensitive multiplexed in vivo imaging using pegylated upconversion nanoparticles. *Nano Res*. 2010;3:722–732. doi:10.1007/s12274-010-0036-2.
40. Cooper CR, Chay CH, Pienta KJ. The role of alpha(v)beta(3) in prostate cancer progression. *Neoplasia*. 2002;4(3):191–194. doi:10.1038/sj/neo/7900224.
41. Liapis H, Flath A, Kitazawa S. Integrin alpha V beta 3 expression by bone-residing breast cancer metastases. *Diagn Mol Pathol*. 1996;5(2):127–135.
42. Schnell O, Krebs B, Wagner E, et al. Expression of integrin alphavbeta3 in gliomas correlates with tumor grade and is not restricted to tumor vasculature. *Brain Pathol*. 2008;18(3):378–386. doi:10.1111/j.1750-3639.2008.00137.x.
43. Sloan EK, Pouliot N, Stanley KL, et al. Tumor-specific expression of alphavbeta3 integrin promotes spontaneous metastasis of breast cancer to bone. *Breast Cancer Res*. 2006;8(2):R20. doi:10.1186/bcr1398.
44. Liapis H, Adler LM, Wick MR, Rader JS. Expression of alpha(v)-beta3 integrin is less frequent in ovarian epithelial tumors of low malignant potential in contrast to ovarian carcinomas. *Hum Pathol*. 1997;28(4):443–449.
45. Ruoslahti E, Pierschbacher MD. Arg-Gly-Asp: a versatile cell recognition signal. *Cell*. 1986;44(4):517–518.
46. Dayam R, Aiello F, Deng J, et al. Discovery of small molecule integrin alphavbeta3 antagonists as novel anticancer agents. *J Med Chem*. 2006;49(15):4526–4534. doi:10.1021/jm051296 s.
47. Montenegro JM, Grazu V, Sukhanova A, et al. Controlled antibody/(bio-) conjugation of inorganic nanoparticles for targeted delivery. *Adv Drug Deliv Rev*. 2013;65(5):677–688. doi:10.1016/j.addr.2012.12.003.
48. Xiong L, Yang T, Yang Y, Xu C, Li F. Long-term in vivo biodistribution imaging and toxicity of polyacrylic acid-coated upconversion nanophosphors. *Biomaterials*. 2010;31(27):7078–7085. doi:10.1016/j.biomaterials.2010.05.065.